Nanoparticle and Solution Doping for Efficient Holmium Fiber Lasers

(Invited Paper)

Michal Kamrádek
Ivan Kašík
Jan Aubrecht
Jan Mrázek
Ondrej Podrazký
Jakub Cajzl
Petr Vařák
Vaclav Kubeček
Pavel Peterka
Pavel Honzátko
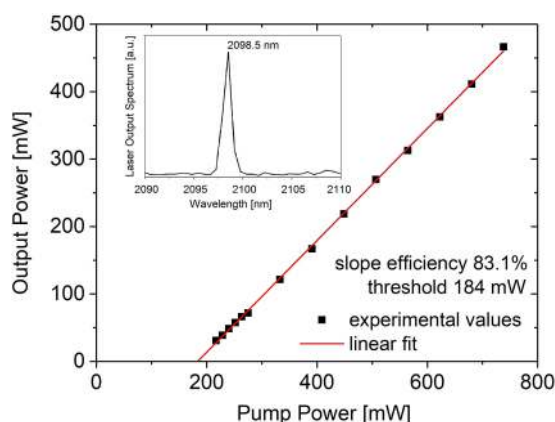
Nanoparticle and Solution Doping for Efficient Holmium Fiber Lasers

(Invited Paper)

Michal Kamrádek [ID],[1,2] **Ivan Kašík,**[1] **Jan Aubrecht** [ID],[1] **Jan Mrázek** [ID],[1]
Ondrej Podrazký,[1] **Jakub Cajzl,**[1,3] **Petr Vařák,**[1,3] **Vaclav Kubeček,**[2]
Pavel Peterka [ID],[1] **and Pavel Honzátko** [ID] [1]

[1]Institute of Photonics and Electronics, Czech Academy of Sciences, 182 51 Prague, Czech Republic
[2]Faculty of Nuclear Sciences and Physical Engineering, Czech Technical University in Prague, Prague 115 19, Czech Republic
[3]University of Chemistry and Technology Prague, 166 28 Prague, Czech Republic

Abstract: Efficient holmium fiber lasers have been studied as attractive laser sources operating around 2.1 μm. We report on holmium-doped silica fibers prepared by the modified chemical vapor deposition in combination with either a solution-doping method or a nanoparticle-doping method. A set of 15 fibers with various compositions was characterized and compared with respect to their fluorescence lifetime, laser slope efficiency and laser threshold. This set of fibers in wide concentration ranges allowed us to assess reliably the influence of material composition and the influence of doping method. The best-performance fibers exhibited slope efficiency 83.1%, laser threshold 155 mW and a record value of upper laser level lifetime of 1.35 ms. These results were achieved in fibers with holmium concentration lower than 800 molar ppm and Al/Ho molar ratio greater than 70. Significant differences between fibers prepared by solution doping and nanoparticle doping were not observed. The behavior of Al_2O_3 nanoparticles during fiber preparation is discussed in details.

Index Terms: Fiber laser, infrared fibers.

1. Introduction

Holmium-Doped optical fibers have been recently studied for a use in fiber lasers emitting in the range 2.05–2.2 μm [1]–[4]. In the question of a host matrix, silica glass belongs among appropriate options. Its material parameters such as transparency, thermal stability and chemical durability remain unmatched. The compatibility with common fiber components is also worth mentioning. On the other hand, silica's main drawbacks lie in high phonon energy and low solubility of rare-earths (RE). To overcome these deficiencies, pure silica needs to be co-doped with suitable modifiers. For applications in fiber lasers, aluminum oxide is particularly beneficial [5]–[7]. Using the Modified Chemical Vapor Deposition (MCVD) method [8], fibers are commonly co-doped through the well-known solution-doping (SD) technique [9]. An alternative approach using a dispersion of nanoparticles is called a nanoparticle-doping (NP) method.

The use of nanoparticles implemented into MCVD for erbium-doped glasses was noted by Le Sauze *et al.* already in 2003 [10]. However, no specifications about the nanoparticles or the doping

process were given. The use of alumina nanoparticles in optical fiber preparation was for the first time reported in details by Podrazký *et al.* in 2007 [11]. The authors used alumina nanoparticles to lower the matrix phonon energy in erbium ions vicinity and to prevent clustering. They found the nanoparticles lower fiber attenuation and increase erbium emission in fiber amplifiers. Moreover, they proposed future utilization of mixed Al-Er and Al-Tm oxide nanoparticles in fibers preparation.

Since this pioneering work, the nanoparticle-doping technique has been extensively developed and practically substituted solution doping for various applications [12]–[16]. Nowadays, nanoparticles are widely used in the preparation of active optical fibers doped with erbium [15], [17], terbium [18], europium [18], holmium [19] and thulium [20]. Many variations were reported also in nanoparticles composition. Besides Al_2O_3, nanoparticles of various oxides ($Y_3Al_5O_{12}$ [20], Lu_2O_3 [19]) and fluorides (LaF_3 [18], alkaline-earth fluorides [21]) have been described. In combination with MCVD, commercial powders [11] as well as co-precipitated precursors [13] can be used. Alternative methods of nanostructures formation in various oxide systems during preform thermal annealing have also been published [22]–[25].

The NP approach is generally considered to give improved laser characteristics than the SD one [7], [26] although excellent results were obtained also with solution-doped fibers [27]–[31]. General opinion preferring NP to SD is based on the idea that nanoparticles form optimized submicron local environment around RE ions, and thus improve their fluorescence characteristics [14], [21]. Appropriate nanoparticles lower phonon energy of the silica matrix and keep fluorescent RE ions more distant leading to decreased pair-induced quenching and suppression of up-conversion processes. But, the assumption of beneficial RE local environment can be met only in the case of nanoparticles stability during thermal treatment. Taking into account the temperatures of silica processing, around 2000 °C, the stability of commonly used nanoparticles cannot be guaranteed. There exist a serious risk of nanoparticles decomposition during preform fabrication leading to a formation of new phases. Several studies on fluoride [32], [33] as well as oxide [34] nanoparticles have been already published. The reaction of alumina with silica has been described in details by Takahashi and Matsushima [35]. Possible structural changes needs to be taken into account also during fiber drawing when the cooling rate is a several hundred degrees per second [36].

Several comparisons of SD vs. NP methods, considering fluorescence lifetime and lasing characteristics, have been reported so far [16], [17], [19], [26], [37], [38]. Nevertheless, in most cases, complex effects of fiber composition on the properties were not taken into account. For example, the decrease of fluorescence lifetime with increasing RE concentration [39] and decreasing co-dopant concentration [20] is frequently neglected. In order to compare thoroughly both discussed doping techniques, these influences need to be carefully separated.

For practical technological reasons, it is nearly impossible to prepare at least one pair of optical fibers with exactly the same composition by both techniques. Our approach is based on multiple samples in wide concentration ranges. In this case, it is possible to determine the influence of material composition and the influence of doping method.

In this paper, we deal with holmium-doped silica fibers co-doped with alumina for fiber lasers. We bring a broad survey of solution-doping and nanoparticle-doping techniques. The study was done on 15 samples, 7 prepared by SD and 8 by NP, with various dopant concentration ranges. The fibers were compared from the point of view of fluorescence lifetime, laser threshold and laser slope efficiency. We found the best characteristics in fibers with low Ho^{3+} concentration and high Al/Ho ratio. Our results may help with designing of advanced holmium-doped silica optical fibers.

2. Experimental

In order to examine the influence of preparation method in detail, we prepared two sets of optical fibers with alumina and holmium in wide concentration ranges. One series was processed through the solution-doping method while the other one through the nanoparticle-doping method. The fibers were compared according to their fluorescence lifetimes and laser characteristics.

2.1 Preparation of Preforms and Optical Fibers

The fibers were drawn from optical preforms prepared by the MCVD process. The preforms were co-doped with holmium and aluminum either by the SD or by the NP method. Pure silica tubes (F300, Heraeus) with 18 mm outer diameter and 1.4 mm wall thickness were used as substrates. Extra pure $SiCl_4$ (FO Optipur, Merck) and onsite purified O_2 (dew point <-90 °C) were used as SiO_2 precursors. At first, we polished the deposition tube at 2000 °C and deposited two buffer SiO_2 layers. Thereafter, we deposited one porous core layer, called a frit, which was subsequently soaked with the doping medium. After drying and sintering, the tube was collapsed into the optical preform. The sintering was done under a chlorine atmosphere generated by thermal decomposition of carbon tetrachloride inside the tube.

In the SD process, the frits were soaked with an ethanolic (99.9%, VWR) solution of aluminum chloride ($AlCl_3$ anhydrous, 99.999%, Sigma-Aldrich) and holmium (III) chloride ($HoCl_3 \cdot 6H_2O$, 99.99%, Sigma-Aldrich). The solution was then drained out of the tube and doped frit was dried. Finally, the frit was sintered and collapsed into the preform.

In the case of NP process, a doping suspension was used. The suspension consisted of holmium (III) chloride ($HoCl_3 \cdot 6H_2O$, 99.99%, Sigma-Aldrich) and aluminum oxide nanoparticles of <50 nm size (γ-Al_2O_3, 99.9%, Sigma-Aldrich) in absolute ethanol (99.9%, VWR). The suspension was freshly sonicated before use in order to minimize the risk of nanoparticles agglomeration. After soaking, the frit was, dried, sintered and collapsed into the preform.

Optical fibers were drawn at a 6 m high tower of our own construction at a temperature of 1950 °C. The fibers had cladding diameter of 125 μm (precision $\pm$ 1 μm) and core diameter of approximately 10 μm. Fibers were coated during drawing with a UV-curable acrylate (Cablelite 3471-3-14, DSM Functional Materials). The coating thickness was about 75 μm.

2.2 Preforms and Fibers Characterization Methods

A Photon Kinetics A2600 refractive index profiler was used to measure refractive index profiles (RIP) of the preforms. To verify the preform longitudinal homogeneity, the RIPs were determined at several longitudinal positions under nine angles in each position. Averaged profiles were calculated and compared. The RIPs were confirmed in fibers using an IFA-100 profiler (Interfiber Analysis).

Dopant concentration profiles were obtained by electron probe microanalysis (EPMA) using a Cameca-SX100. Polished preform cross-cuttings were analyzed in 20 equidistant points across the core and averaged values were calculated.

The fibers were characterized given to their spectral absorption. We used several set-ups to determine background losses, hydroxyl content and holmium ion concentration. In all cases, a tungsten halogen lamp was used as a broadband source of radiation. The background losses were measured by the standard cutback method [40] using an Ando AQ1425 optical spectrum analyzer. The losses were evaluated from absorption minima at around 1300 nm. Hydroxyl contents were calculated based on the absorption peak at 1383 nm [41], [42]. Holmium ion concentrations were determined from absorption spectra measured with a Nicolet 8700 Fourier-transform infrared spectrometer (spectral range 1000–2500 nm, resolution 16 cm^{-1}). The main absorption peak at 1950 nm, corresponding to the $^5I_8 \rightarrow ^5I_7$ electron transition, was used for calculation. The Ho^{3+} concentration N^{Ho} [ions·m^{-3}] was calculated from the peak absorption value A [dB·m^{-1}] based on (1). The absorption cross section σ_a at the peak ground state absorption was $2.954 \cdot 10^{-25}$ m^2 and the overlap factor was considered to be $\Gamma = 1$ for simplicity. Because of the fact that the real values of the overlap factor are slightly lower than unity, calculated values N^{Ho} are considered as lower limits of the actual concentrations.

$$A = 4.34 \cdot \sigma_a \cdot N^{Ho} \cdot \Gamma \qquad (1)$$

The emission spectra were measured in an experimental setup consisted of a thulium-doped fiber laser emitting at 1950 nm, an optical isolator and an optimized broadband optical coupler. Reflected radiation was eliminated with angle-polished connectors terminating the fiber components. The emission spectra were collected by a Fourier-transform infrared spectrometer in the wavelength
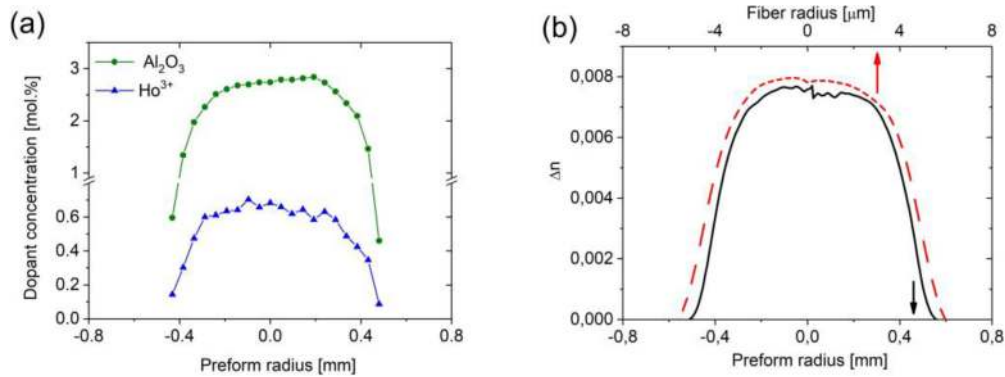
Fig. 1. (a) Dopant profiles in preform NP1558, (b) Refractive index profiles of NP1558 preform and fiber.

range 1750–2250 nm with the resolution of 4 cm^{-1}. The spectra were carefully corrected for the insertion loss of the wideband coupler and for the sensitivity of InGaAs photodetector [43].

Fluorescence lifetimes were measured according to a side detection setup. Decay curves measured for various pump powers from the side of the stripped fiber were recorded and analyzed. The decays were normalized and a time value at the 1/e point was determined as the fluorescence lifetime. The lifetimes were extrapolated to the zero pump power to eliminate the detrimental effect of amplified spontaneous emission. Detailed description of the fluorescence lifetime measurement has been already published elsewhere [37], [43].

2.3 Fiber Laser Setup

The fibers were tested in a Fabry-Perot laser configuration. The laser setup is depicted in Fig. 3(a). The setup was based on an in-house prepared thulium-doped fiber (TDF) pumped by a ring fiber laser at 1565 nm. The ring laser consisted of a commercial erbium/ytterbium-doped double-clad fiber (Er/Yb-DCF), an optical coupler (OC), an optical isolator (ISO) and a pump and signal combiner. The cavity was formed by fiber Bragg gratings (FBG) with low reflectivity (LR) and high reflectivity (HR) at 1950 nm. The maximum output power at 1950 nm was approximately 1 W. The performance of holmium-doped fibers (HDF) was tested in a cavity formed by HRFBG at 2100 nm (R∼99.5%) and perpendicularly cleaved fiber end (R∼3.5%). A power meter Gentec Turner XLP12-3S-H2-D0 was used to measure the laser output power. Custom-made (Crytur) filters with 99% reflectivity at 1950 nm and 90.5% transmission at 2100 nm were used to separate the pump and signal power. In order to find the optimal fiber length, tested fibers were gradually shortened and characterized. For each fiber length, laser threshold and slope efficiency with respect to the absorbed pump power were determined. Holmium laser spectra were monitored with a Miriad S3 spectrometer (integration time 20 μs, resolution 2 nm).

3. Results and Discussion

The distributions of dopants in the preform NP1558 is depicted in Fig. 1(a). These concentration profiles are shown as a typical example, all of the samples showed similar shapes. The profiles of Al_2O_3 and Ho^{3+} were homogenous with a flat maximum in the center. Corresponding RIPs of preform and fiber NP1558 can be seen in Fig. 1(b), the profiles are well comparable.

Background losses were found to be in the range 10–40 dB/km in all of the fibers, hydroxyl content was 1–2 molar ppm. We find these values appropriate to the fabrication methods and low enough not to have any significant detrimental effects on laser characteristics [44].

Representative $^5I_8 \leftrightarrow {}^5I_7$ absorption and emission spectra of the holmium-doped fibers are shown in Fig. 2. The spectral shape of absorption and emission corresponds well to the holmium spectra
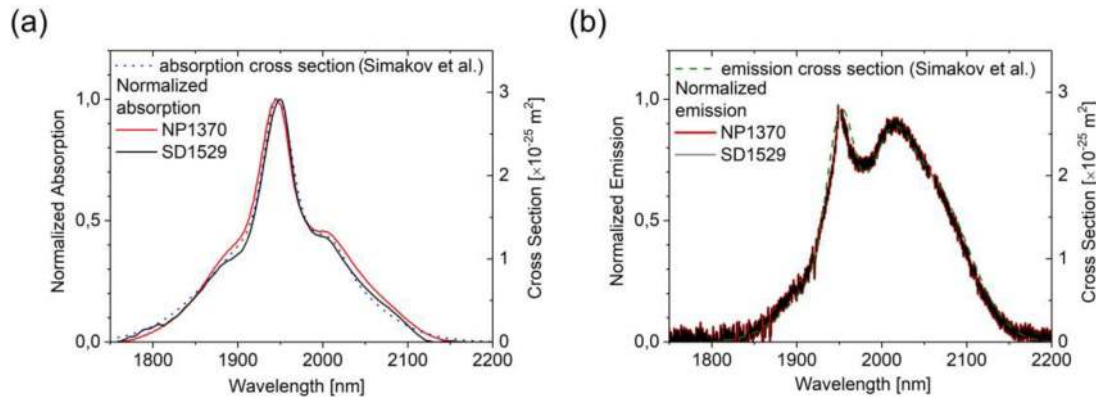
Fig. 2. Measured spectral shape of (a) absorption and (b) emission in representative fiber samples. Absorption and emission cross sections reported by Simakov *et al.* [45] are added for comparison.
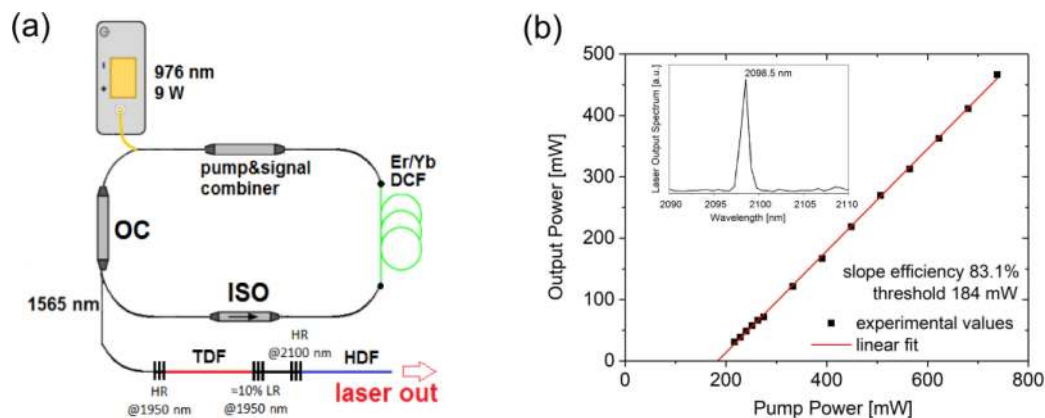

Fig. 3. (a) Fiber laser setup and (b) linear fit of laser data, inset laser spectrum.

in an aluminosilicate host material reported in literature [45]. It should be noted that the emission published there was estimated from the absorption spectrum by McCumber theory.

Laser data and laser spectrum measured with the optimal fiber length of NP1544 are depicted in Fig. 3(b). The data were fitted linearly and threshold and slope were calculated. The laser spectrum was centered at 2100 nm (with respect to spectrometer resolution) in accordance with the used HRFBG. The optimized fiber lengths L_{opt} were in all of the fibers in the order of meters.

The relevant parameters of prepared preforms and fibers are summarized in Table 1. Preforms labeled SD were prepared via solution doping and preforms labeled NP were prepared via nanoparticle doping.

Taking into account small dopant fluctuations along the preforms and the accuracies of EPMA and absorption measurements, we can say that both sets of Ho^{3+} concentrations are in excellent agreement and can be considered as reliable values. The Al/Ho ratios were calculated from EPMA data which were measured in the same position. On the other hand, lifetimes and laser characteristics are related to the concentrations obtained from absorption measurements because these experiments were performed with identical fiber pieces.

3.1 Fluorescence Lifetime

Measured fluorescence lifetimes can be found in Fig. 4. The highest lifetimes are well above 1000 μs. The value of 1348 μs represents, to the best of our knowledge, a record lifetime measured

TABLE 1
Relevant Parameters of Studied Fibers

| Sample	Al_2O_3 [mol.%]	Ho^{3+} [ppm] EPMA	Ho^{3+} [ppm] absorption	Al/Ho	Fluorescence lifetime [μs]	Slope [%]	Threshold [mW]	L_{opt}
SD1294	3.17	560	501	113.2	1217	77.0	165	6.3
SD1524	1.3	712	869	36.5	923	72.2	517	3.0
SD1370	4.30	970	680	88.7	1348	76.6	155	3.3
SD1347	3.97	1850	1333	42.9	986	72.0	372	2.4
SD1412	1.26	2440	2674	10.3	764	49.1	604	1.0
SD1543	2.40	2490	2493	19.3	869	56.4	367	1.0
SD1348	3.19	3200	3184	19.9	815	51.1	519	0.8
NP1551	2.57	436	433	117.9	1152	76.5	264	6.0
NP1544	3.50	633	631	110.6	1280	83.1	184	4.3
NP1529	2.43	680	740	71.5	1168	77.5	312	3.0
NP1557	2.87	1177	1059	48.8	1035	74.5	271	2.2
NP1370	3.33	1510	1874	44.1	890	60.7	363	1.5
NP1542	2.38	1706	1942	27.9	946	66.9	361	1.3
NP1559	2.76	2143	1408	25.8	1013	73.8	263	1.8
NP1558	2.35	5490	4687	8.6	805	41.8	561	0.6
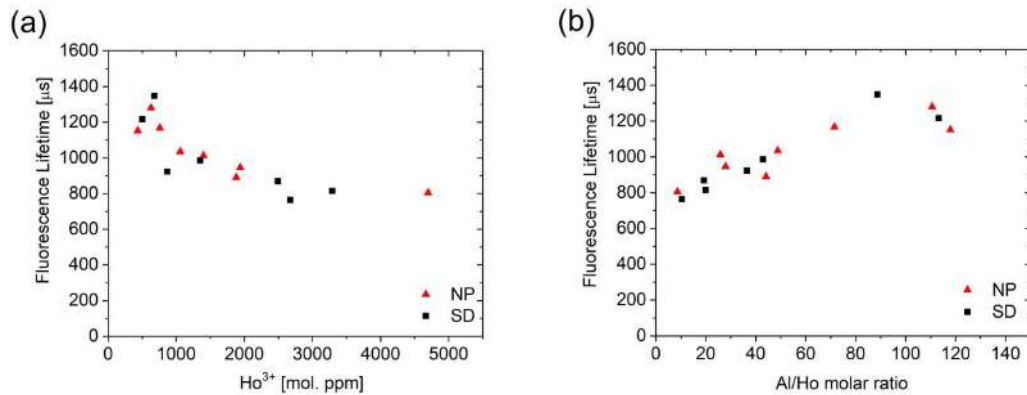
Fig. 4. Fluorescence lifetime as a function of (a) Ho^{3+} concentration and (b) Al/Ho molar ratio.

for the $^5I_7$ level in holmium-doped silica-based fibers. As can be seen, the highest lifetimes were achieved in fibers with Ho^{3+} concentration under ∼800 mol. ppm and Al/Ho molar ratio greater than 70. The decrease in lifetime with either increasing Ho^{3+} concentration or decreasing Al/Ho ratio can be attributed to energy transfer up-conversion and cross-relaxation processes. The beneficial effect of increased Al/RE ratio on fluorescence intensity was observed already by Arai *et al.* in neodymium-doped silica glass [5] and by Faure *et al.* in the case of lifetimes of thulium-doped silica fibers [7].

3.2 Slope Efficiency

Graphs for the slope efficiencies are depicted in Fig. 5. The highest efficiencies around 80% were obtained with Ho^{3+} concentrations lower than ∼800 mol. ppm and Al/Ho molar ratio greater than 70. These values correspond to around 86% of the theoretical maximum. The excellent slope efficiency of 83.1%, more than 89% of the theoretical efficiency, was achieved in the fiber SD1370. As was already stated by Wang *et al.* [44], such high efficiencies were reported only rarely. The record
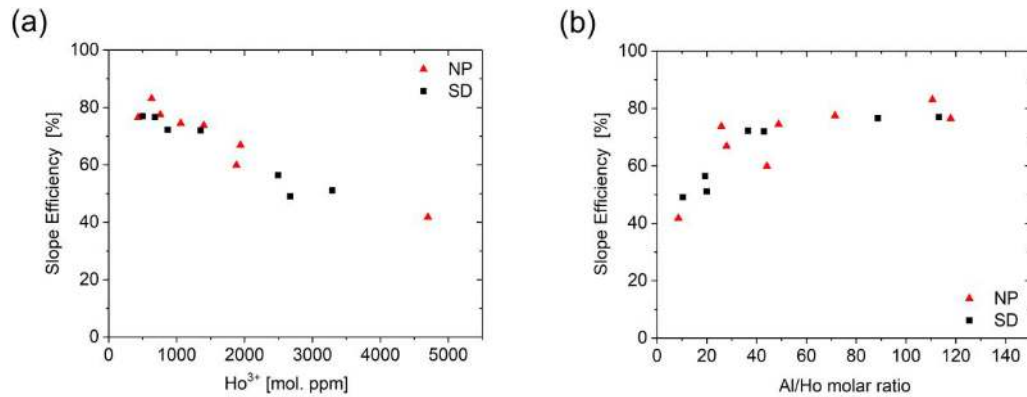
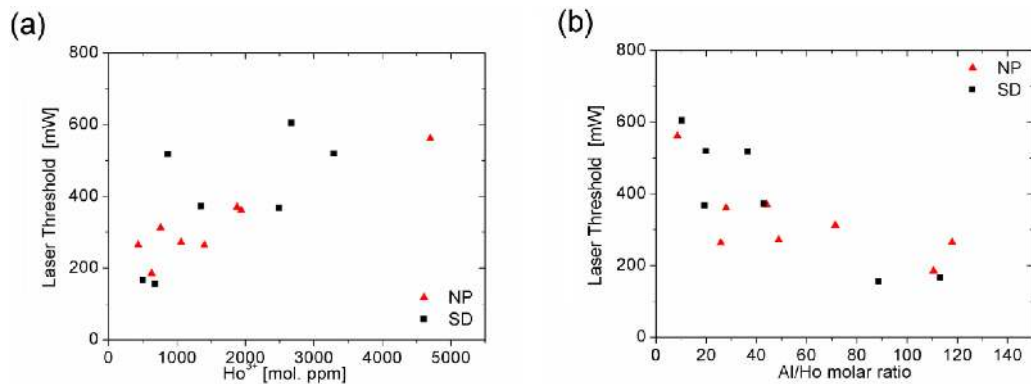Fig. 5. Laser slope efficiency as a function of (a) Ho^{3+} concentration and (b) Al/Ho molar ratio.

Fig. 6. Laser threshold as a function of (a) Ho^{3+} concentration and (b) Al/Ho molar ratio.

slope efficiency, 93% of the maximum theoretical value, was published by Heming *et al.* [46] in 2016. The lower than theoretical efficiencies can be ascribed to a strong tendency of holmium ions to form clusters even at low Ho^{3+} concentrations [44]. For the best performances, some studies also predicted the necessity of OH^- contamination below 1 ppm [29], [45]. The reduced efficiency with increasing Ho^{3+} content and decreasing Al/Ho ratio can be ascribed to the energy transfer up-conversion and cross-relaxation processes.

Similar dependencies were observed by Baker *et al.* in erbium-doped fibers [17]. The authors reported the highest slope efficiencies for fibers with Er^{3+} concentration under $2.22 \cdot 10^{25}$ ions·m^{-3} (cca 1000 mol. ppm) and Al/Er ratio of 50. This group presented also high efficiencies (around 75%) in holmium-doped fibers with Ho^{3+} concentrations of thousands of ppm (up to ~4500 ppm) [31]. In these cases, the Al/Ho ratio was kept 30–50. Apparently, the Al/Ho ratio has stronger effect than the absolute Ho^{3+} concentration. Note their fibers were of very low OH^- content, <0.5 ppm.

3.3 Laser Threshold

The values of laser threshold can be found in Fig. 6. The data for threshold are a little bit more scattered than for lifetime and slope efficiency nevertheless the trends can be clearly seen. The laser threshold increases with Ho^{3+} concentration while its dependence on Al/Ho ratio shows an indirect proportion. Quite low laser thresholds, well under 200 mW, were achieved for Ho^{3+} concentrations under ~800 mol. ppm and for Al/Ho ratio greater than 80. In holmium-doped silica fibers, such low values have not been published yet.

A quite surprising and important fact is that no significant differences between SD and NP fibers were observed. It is well evident in all of the graphs above that no beneficial effect of nanoparticles on lifetime or laser characteristics can be found. Presented dependencies have the same shapes for the SD as well as for the NP samples. These findings are in agreement with results reported by Vermillac et al. [20] in the case of lifetimes in lanthanum-doped thulium fibers. Also Baker et al. presented such a results for lifetimes in erbium-doped fibers [17].

This phenomenon can be explained by the fact that alumina nanoparticles are decomposed under a heat treatment during fiber preparation. The reaction of Al_2O_3 with SiO_2 in bulk samples was described by Cajzl et al. [34] and Takahashi and Matsushima [35]. Their results clearly demonstrate the formation of mullite phase, $3Al_2O_3 \cdot 2SiO_2$, at temperatures above 1200 °C. Both studies confirm the data based on alumina-silicate phase diagram [47]. The decomposition of Al_2O_3 nanoparticles in borosilicate glass was also observed [48].

To summarize the results, the best properties were obtained in fibers with the Al/Ho molar ratio greater than 70. It should be noted that the optimal ratio can be estimated from the fundamentals of solid state chemistry. Assuming the mullite phase formation during fiber preparation, Ho^{3+} ions can be located either inside it or outside, in the glass matrix. Based on the crystal-chemistry approach [49], location inside the mullite phase would be preferred and beneficial for increased lifetimes. Rare-earth ions dissolved in the silica matrix are quenched rapidly and provide very short lifetimes [5]. However, the maximum rare-earth concentration in mullite is limited. Unfortunately, the concentration limits have not been studied exactly yet. A comprehensive review can be found in [50]. The maximum rare-earth concentration in the mullite phase was published by Wang et al. [51] in the case of terbium-doped mullite. Based on their data, the optimized composition contained 8 mol.% of Tb^{3+} which gives the Al/Tb ratio equal to 75. This value agrees well with our findings as well as with the data reported by Baker et al. in the case of erbium-doped fibers [17]. The authors found the best results for Al/Er molar ratio of 50 although their fibers have not been optimized primarily according to this parameter.

For the design of high-efficiency optical fibers, it needs to be kept in mind that the fiber preparation is a complex process which significantly changes the chemical and structural properties of starting materials. Since the dopant concentrations are usually at the edge of detection limits of conventional structural analyzers, the exact phase identification remains a challenging task of a material research. Our results attract more attention on this problematics.

4. Conclusions

We have reported holmium-doped silica fibers for a use in fiber lasers. With samples in wide concentration ranges of holmium and Al/Ho molar ratios, we have demonstrated the dependencies of fluorescence lifetime, slope efficiency and laser threshold on the fiber composition. We have reported fibers with fluorescence lifetimes longer than 1000 μs and slope efficiencies around 80%. The longest measured fluorescence lifetime of 1348 μs means, to the best of our knowledge, a record in holmium-doped silica fibers. The slope efficiencies rank among the highest currently published values. We were able to obtain laser threshold as low as 155 mW. Such a low value in holmium-doped silica fibers have not been published yet. We have clearly demonstrated the strong dependence of studied characteristics on the holmium concentration and Al/Ho ratio. The best characteristics were achieved with holmium concentration under 800 molar ppm and Al/Ho molar ratio greater than 70. Compared to already published data, it seems that the Al/RE molar ratio, not the absolute RE concentration, is the crucial parameter.

Characteristics measured with the fibers prepared via solution doping and via nanoparticle doping did not exhibit significant differences and followed the same trends varying only within random variations. This can be attributed to the fact that alumina nanoparticles react with the silica matrix during thermal processing giving the same holmium vicinity as formed during solution doping. Our results find utilization in the designing of advanced optical fibers for high-power fiber lasers.

References

[1] A. Hemming, N. Simakov, J. Haub, and A. Carter, "A review of recent progress in holmium-doped silica fibre sources," *Opt. Fiber. Technol.*, vol. 20, pp. 621–630, 2014.

[2] S. D. Jackson, "Midinfrared holmium fiber lasers," *IEEE J. Quantum Electron.*, vol. 42, no. 2, pp. 187–191, Feb. 2006.

[3] L. G. Holmen *et al.*, "Tunable holmium-doped fiber laser with multiwatt operation from 2025 nm to 2200 nm," *Opt. Lett.*, vol. 44, pp. 4131–4134, 2019.

[4] A. V. Kir'yanov, Y. O. Barmenkov, I. L. Villegas-Garcia, J. L. Cruz, and M. V. Andres, "Highly efficient holmium-doped all-fiber ~2.07-μm laser pumped by ytterbium-doped fiber laser at ~1.13 μm," *IEEE J. Sel. Top. Quantum Electron.*, vol. 24, no. 5, Sep./Oct. 2018, Art. no. 0903108.

[5] K. Arai, H. Namikawa, K. Kumata, T. Honda, Y. Ishii, and T. Handa, "Aluminum or phosphorus co-doping effects on the fluorescence and structural properties of neodymium-doped silica glass," *J. Appl. Phys.*, vol. 59, pp. 3430–3436, 1986.

[6] J. Kirchhof, S. Unger, A. Schwuchow, S. Jetschke, and B. Knappe, "Dopant interactions in high-power laser fibers," *Proc. SPIE*, vol. 5723, pp. 261–272, 2005.

[7] B. Faure, W. Blanc, B. Dussardier, and G. Monnom, "Improvement of the Tm^{3+}:$^3H_4$ level lifetime in silica optical fibers by lowering the local phonon energy," *J. Non-Cryst. Solids*, vol. 353, pp. 2767–2773, 2007.

[8] S. R. Nagel, J. B. Macchesney, and K. L. Walker, "An overview of the modified chemical vapor deposition (MCVD) process and performance," *IEEE J. Quantum Electron.*, vol. QE-18, no. 4, pp. 459–476, Apr. 1982.

[9] J. E. Townsend, S. B. Poole, and D. N. Payne, "Solution-doping technique for fabrication of rare-earth-doped optical fibers," *Electron. Lett.*, vol. 23, pp. 329–331, 1987.

[10] A. Le Sauze *et al.*, "Nanoparticle doping process: Towards a better control of erbium incorporation in MCVD fibers for optical amplifiers," *Opt. Amplifiers Their Appl.*, 2003, Art. no. WC5.

[11] O. Podrazky, I. Kasik, M. Pospisilova, and V. Matejec, "Use of alumina nanoparticles for preparation of erbium-doped fibers," in *Proc. IEEE Lasers Electro-Opt. Soc. Annu. Meeting Conf.*, 2007, vol. 1/2, pp. 246–247.

[12] O. Podrazky, I. Kasik, M. Pospisilova, and V. Matejec, "Use of nanoparticles for preparation of rare-earth doped silica fibers," *Phys. Status Solidi C*, vol. 6, no. 10, pp. 2228–2230, 2009.

[13] A. Pastouret *et al.*, "Nanoparticle doping process for improved fibre amplifiers and lasers," *Proc. SPIE*, vol. 7195, 2009, Art. no. 71951X.

[14] D. Boivin *et al.*, "Performance characterization of new erbium-doped fibers using MCVD nanoparticle doping process," *Proc. SPIE*, vol. 7914, 2011, Art. no. 791423.

[15] I. Kasik *et al.*, "Erbium and Al_2O_3 nanocrystals-doped silica optical fibers," *Bull. Pol. Acad. Sci.-Tech. Sci.*, vol. 62, pp. 641–646, 2014.

[16] C. C. Baker *et al.*, "Nanoparticle doping for improved Er-doped fiber lasers," *Proc. SPIE*, vol. 9728, 2016, Art. no. 97280T.

[17] C. C. Baker *et al.*, "Nanoparticle doping for high power fiber lasers at eye-safer wavelengths," *Opt. Exp.*, vol. 25, pp. 13903–13915, 2017.

[18] C. Kucera *et al.*, "Designer emission spectra through tailored energy transfer in nanoparticle-doped silica preforms," *Opt. Lett.*, vol. 34, pp. 2339–2341, 2009.

[19] E. J. Friebele *et al.*, "Ho-nanoparticle doping for improved high-energy laser fibers," *Proc. SPIE*, vol. 10100, 2017, Art. no. 1010003.

[20] M. Vermillac *et al.*, "Thulium-doped nanoparticles and their properties in silica-based optical fibers," *Proc. SPIE*, vol. 10683, 2018, Art. no. 106831F.

[21] T. Lindstrom *et al.*, "Spectral engineering of optical fiber preforms through active nanoparticle doping," *Opt. Mater. Exp.*, vol. 2, pp. 1520–1528, 2012.

[22] A. V. Kir'yanov *et al.*, "Fabrication and characterization of new Yb-doped zirconia-germano-alumino silicate phase-separated nano-particles based fibers," *Opt. Exp.*, vol. 19, pp. 14823–14837, 2011.

[23] M. C. Paul *et al.*, "Yb_2O_3 doped yttrium-alumino-silicate nano-particles based LMA optical fibers for high-power fiber lasers," *J. Light. Technol.*, vol. 30, no. 13, pp. 2062–2068, Jul. 2012.

[24] M. C. Paul, A. Dhar, S. Das, A. A. Latiff, M. T. Ahmad, and S. W. Harun, "Development of nanoengineered thulium-doped fiber laser with low threshold pump power and tunable operating wavelength," *IEEE Photon. J.*, vol. 7, no. 1, Feb. 2015, Art. no. 7100408.

[25] J. Duarte *et al.*, "Optical amplification performance of erbium doped zirconia-yttria-alumina-baria silica fiber," *Opt. Mater. Exp.*, vol. 9, pp. 2652–2661, 2019.

[26] E. J. Friebele *et al.*, "Erbium nanoparticle doped fibers for efficient, resonantly-pumped Er-doped fiber lasers," *Proc. SPIE*, vol. 9344, 2015, Art. no. 934412.

[27] S. D. Jackson and S. Mossman, "Efficiency dependence on the Tm^{3+} and Al^{3+} concentrations for Tm^{3+}-doped silica double-clad fiber lasers," *Appl. Opt.*, vol. 42, pp. 2702–2707, 2003.

[28] A. S. Kurkov *et al.*, "Holmium fiber laser based on the heavily doped active fiber," *Laser Phys. Lett.*, vol. 6, pp. 661–664, 2009.

[29] E. J. Friebele *et al.*, "Ho-doped fiber for high energy laser applications," *Proc. SPIE*, vol. 8961, 2014, Art. no. 896120.

[30] D. Pal, A. Dhar, R. Sen, and A. Pal, "All-fiber holmium laser at 2.1 μm under in-band pumping," in *Proc. 13th Int. Conf. Fiber Opt. Photon.,* Kanpur, India, 2016, Art. no. Tu3E.2.

[31] C. C. Baker *et al.*, "Recent advances in holmium doped fibers for high-energy lasers (Conference Presentation)," *Proc. SPIE*, vol. 10637, 2018, Art. no. 1063704.

[32] J. DiMaio, B. Kokuoz, T. L. James, T. Harkey, D. Monofsky, and J. Ballato, "Photoluminescent characterization of atomic diffusion in core-shell nanoparticles," *Opt. Exp.*, vol. 16, pp. 11769–11775, 2008.

[33] M. Vermillac *et al.*, "Use of thulium-doped LaF_3 nanoparticles to lower the phonon energy of the thulium's environment in silica-based optical fibres," *Opt. Mater.*, vol. 68, pp. 24–28, 2017.

[34] J. Cajzl *et al.*, "The influence of nanostructured optical fiber core matrix on the optical properties of EDFA," *Proc. SPIE*, vol. 8775, 2013, Art. no. 877509.

[35] H. Takahashi and Y. Matsushima, "Investigation on luminescent properties of rare earth doped mullite phosphors and the occupation site of the doped rare earths," *J. Electrochem. Soc.*, vol. 166, pp. B3209–B3217, 2019.

[36] M. Vermillac *et al.*, "Fiber-draw-induced elongation and break-up of particles inside the core of a silica-based optical fiber," *J. Amer. Ceram. Soc.*, vol. 100, pp. 1814–1819, 2017.

[37] M. Kamrádek *et al.*, "Spectroscopic characterization of holmium-doped optical fibers for fiber lasers," *Proc. SPIE*, vol. 11029, 2019, Art. no. 1102908.

[38] M. Kamrádek *et al.*, "Thulium-doped optical fibers for fiber lasers," *Proc. SPIE*, vol. 10603, 2017, Art. no. 106030V.

[39] M. Kamrádek *et al.*, "Spectral properties of thulium doped optical fibers for fiber lasers around 2 micrometers," *Proc. SPIE*, vol. 10232, 2017, Art. no. 1023205.

[40] E. Desurvire, *Erbium-Doped Fiber Amplifiers: Principles and Applications / Emmanuel Desurvire*. New York, NY, USA: Wiley, 1994.

[41] O. Humbach, H. Fabian, U. Grzesik, U. Haken, and W. Heitmann, "Analysis of OH absorption bands in synthetic silica," *J. Non-Cryst. Solids*, vol. 203, pp. 19–26, 1996.

[42] J. Aubrecht *et al.*, "Self-swept holmium fiber laser near 2100 nm," *Opt. Exp.*, vol. 25, pp. 4120–4125, 2017.

[43] J. Cajzl *et al.*, "Thulium-doped silica fibers with enhanced fluorescence lifetime and their application in ultrafast fiber lasers," *Fibers*, vol. 6, 2018, Art. no. 66.

[44] J. C. Wang, N. Bae, S. B. Lee, and K. Lee, "Effects of ion clustering and excited state absorption on the performance of Ho-doped fiber lasers," *Opt. Exp.*, vol. 27, pp. 14283–14297, 2019.

[45] N. Simakov, A. Hemming, W. A. Clarkson, J. Haub, and A. Carter, "A cladding-pumped, tunable holmium doped fiber laser," *Opt. Exp.*, vol. 21, pp. 28415–28422, 2013.

[46] A. Hemming, N. Simakov, M. Oermann, A. Carter, and J. Haub, "Record efficiency of a holmium-doped silica fibre laser," in *Proc. Conf. Lasers Electro-Opt.*, 2016, Art. no. SM3Q.5.

[47] F. J. Klug, S. Prochazka, and R. H. Doremus, "Alumina-silica phase diagram in the mullite region," *J. Amer. Ceram. Soc.*, vol. 70, pp. 750–759, 1987.

[48] J. Massera, L. Petit, J. Koponen, B. Glorieux, L. Hupa, and M. Hupa, "Er^{3+}-Al_2O_3 nanoparticles doping of borosilicate glass," *Bull. Mater. Sci.*, vol. 38, pp. 1407–1410, 2015.

[49] J. Wang, W. S. Brocklesby, J. R. Lincoln, J. E. Townsend, and D. N. Payne, "Local structures of rare-earth ions in glasses: The 'crystal-chemistry' approach," *J. Non-Cryst. Solids*, vol. 163, pp. 261–267, 1993.

[50] H. Schneider, R. X. Fischer, and J. Schreuer, "Mullite: Crystal structure and related properties," *J. Amer. Ceram. Soc.*, vol. 98, pp. 2948–2967, 2015.

[51] G. G. Wang, X. F. Wang, L. W. Dong, and Q. Yang, "Synthesis and photoluminescence of green-emitting Ce^{3+},Tb^{3+} co-doped $Al_6Si_2O_{13}$ phosphors with high thermal stability for white LEDs," *RSC Adv.*, vol. 6, pp. 42770–42777, 2016.